Eur. Phys. J. B **34**, 69–84 (2003)
DOI: 10.1140/epjb/e2003-00198-y

THE EUROPEAN PHYSICAL JOURNAL B

Singular behavior of the Emery model with O-O hopping for high-T_c superconductors

I. Mrkonjić[a] and S. Barišić

Department of Physics, University of Zagreb, Bijenička 32, POB 331, 10002 Zagreb, Croatia

Received 22 March 2002 / Received in final form 30 May 2003
Published online 23 July 2003 – © EDP Sciences, Società Italiana di Fisica, Springer-Verlag 2003

Abstract. Mean field slave boson (MFSB) solution is found analytically for the Emery model of the high-T_c cuprates with infinite interaction U_d on the Cu-site and finite O-O hopping t', in addition to the Cu-O hopping t_0. The solution is found for arbitrary Cu-O charge transfer energy Δ_{pd} and small doping δ, assuming only $t' < 0$ for the insulating phase, appropriate for the superconducting cuprates. It is shown analytically that the Brinkmann-Rice metal-insulator transition is preserved, though shifted to higher values of Δ_{pd}. To the leading order in t', the transition conserves its $t' = 0$ triple point nature with complete electron-hole symmetry with respect to doping. This symmetry is broken by logarithmically small terms related to the t'-induced shift of the chemical potential of the half-filled band from the van Hove singularity. Qualitative change in the behavior of the effective charge transfer energy is found at finite t' for large Δ_{pd}. The prerequisite to MFSB solution is the discussion of the singularities in the 3-band dispersion of the Emery model. The range of parameters leading to the touching of two bands is determined analytically, showing that it is wider than known before. The anticrossing (rather than touching) is however consistent with the observed Fermi surfaces, leading to the MFSB theory with $t' < 0$. The detailed comparison of the theory with the angle-resolved photoemission spectroscopy data in $La_{2-\delta}Sr_\delta CuO_4$, $Bi_2Sr_2CaCuO_{8+\delta}$ and $YBa_2Cu_3O_{7-\delta}$ is finally given, using the properties of the resonant band of the physical fermions, discussed in the companion paper. Fast evolution of the band-structure with doping is explained for LSCO. The three-band fits for Bi2212 and Y123 are equally good, although the Luttinger sum rule is not obeyed there.

PACS. 71.18.+y Fermi surface: calculations and measurements; effective mass, g factor – 74.72.Dn La-based cuprates – 74.25.Jb Electronic structure – 79.60.-i Photoemission and photoelectron spectra

1 Introduction

Long after the discovery of high-T_c cuprates their physical behavior, including the mechanism of high-T_c superconductivity, is not understood [1,2]. Understanding means here that there is an approach which starts with a set of bare particles and their interactions and which, upon renormalization, gives high-T_c superconductivity. At present it is not even known whether a possibly strong [3] electron-phonon interaction is to be included or Coulomb repulsion suffices. In addition, some procedures, like LDA [4], emphasize the multi-band single-particle properties, treating correlations in simplified way, and the others, like the analysis of the Hubbard model [5], insist on accurate correlation effects, but within simplified single-band scheme.

Physically reasonable bridge between these two extremes is provided by the Emery model for the conducting CuO_2 plane [6], which retains three bands, one per Cu or O site in the unit cell. The corresponding tight-binding bare single-particle parameters are the difference between the O and Cu site energies, Δ_{pd}, the Cu-O hopping t_0 and the O-O hopping t'. Various interactions can be added to this model, the largest usually assumed to be the repulsion U_d on copper-site.

Large U_d Emery's model has two principal limits [7]. When $U_d < \Delta_{pd}$ only the lowest, conduction band is appreciably renormalized, i.e. the model reduces to the outright Hubbard case. On the other hand, when $U_d > \Delta_{pd}$, all three bands get involved into the renormalization. The three site structure is conserved at the outset in this, so called (Cu-O) charge-transfer (CT) limit. Actually, within the CT limit two regimes are to be distinguished further, with respect to the location of the doped charge [7]. When it goes to the Cu-site, a Hubbard-like situation is obtained again, whereas when it goes to the O-site, apparently three sites have to be retained. These two limits correspond to the electron ($\delta < 0$) and hole ($\delta > 0$) doping of the CuO_2 planes, respectively. Paraphrasing the above statement,

[a] e-mail: ivanam@phy.hr

the Hubbard-like limit appears for $\delta < 0$ irrespectively of the ratio of U_d and Δ_{pd}, provided that they are sufficiently large with respect to t_0 and t', while for $\delta > 0$ CT nature might prove important. Maximal T_c is achieved upon $\delta > 0$ hole-doping, and this is the regime most often studied [8–10] within the Emery model.

A particulary simple limit, which exhibits the qualitative features described above, takes $U_d > \Delta_{pd}$ CT situation to its $U_d = \infty$ extreme. Large U_d case is usually treated by introducing auxiliary fermion and boson fields [11,12] on the interaction (Cu) site, one of each, when $U_d = \infty$. When the mean-field approximation in the fermion-slave boson (MFSB) decoupling is applied, the three-band structure of the Emery model is obtained with renormalized, effective band-parameters $\Delta_{pd} \to \Delta_{pf}$, $t_0 \to t$, while t' remains non-renormalized [13].

The analytical form of this mapping was found long time ago for $t' = 0$ [7]. The main feature is the Brinkmann-Rice (BR) transition at $\delta = 0$, from the $t = 0$ state at $\Delta_{pd} > 4.74t_0$ to finite t state, below. The transition point is, as emphasized here, the triple point, where the CT $\delta = 0_+$ and the Hubbard-like $\delta = 0_-$ solutions for Δ_{pf} at $\Delta_{pd} > 4.74t_0$ meet unique, finite, t solution for Δ_{pf} at $\Delta_{pd} < 4.74t_0$. On the other hand, for large Δ_{pd}, the effective site energy Δ_{pf} of the 0_+ branch follows the famous $\Delta_{pf} \approx t_0^2/\Delta_{pd}$ [7] asymptotic law, analogous to the behavior of the singlet/triplet site energies in the Zhang-Rice t-J [14] derivative of the Emery model.

The introduction of finite t' into the theory was motivated mainly by two observations. First, t' removes the Fermi energy of the half-filled $\delta = 0$ band from the van Hove (vH) singularity [3,15,16] and opens thus the question of the apparent electron-hole symmetry. Second, t' is important to understand the rotation of the conduction axes from the Cu-O direction to the O-O direction [13], observed by changing the chemical composition of the high-T_c cuprates [17,18]. This led to various numerical solutions of MFSB equations [19–21], usually for very restrictive choices of parameters. But even the most complete numerical calculations [21] have not answered clearly the basic question concerning the stability of $t = 0$ solution at finite t'.

This problem is quite apparent for $\delta = 0_+$ case at large Δ_{pd} when $\Delta_{pf}(t' = 0)$ mentioned above, vanishes after crossing $4|t'|$. As $4|t'|$ is the width of the oxygen band, the effective site energy Δ_{pf} on the Cu-site, if weakly affected by t', enters the O-band. The charge is then transferred to oxygens and the conduction channel $t \neq 0$ is opened. The question of the stability of the $t = 0$ solution is thus related to to the behavior of Δ_{pf} at large Δ_{pd} and finite t'. On the other hand, close to the BR point $t = 0$ stability problem can be rephrased: At finite t' the Fermi level μ_0 of the undoped $\delta = 0$ band is removed from the vH singularity. The same effect occurs at $t' = 0$ by finite doping δ and, as it is well known, makes $t = 0$ solution unstable, suppressing the BR transition. The question is then whether the BR transition persists for $\delta = 0$ and finite t', or it is replaced by a crossover with t always finite. Although the existing numerical calculations suggest [19,21] (but do not prove) that the BR transition on $\Delta_{pd} \approx 4.74t_0$ is conserved, the rigorous proof has to be carried out on very small scale κ_F, measuring the distance of the Fermi level of the half-filled $\delta = 0$ band from the logarithmic vH singularity: $\kappa_F \log|\kappa_F|^{-1} \sim t'/\Delta_{pd}$. A related question concerns the behavior of t and Δ_{pf} around $\Delta_{pd} \approx 4.74t_0$ for finite t', which also requires analytical approach.

The difficulties in treating analytically $t' \neq 0$ problem can be traced back to two facts. The first is that U_d is local (local constraint at $U_d = \infty$), which in the MFSB approximation introduces the integrals over the reciprocal space $\mathbf{k}$. The usual MF minimization before $\mathbf{k}$ integration [7,22] results then in the three coupled integral equations. Second, $\mathbf{k}$ integrals involve only renormalized parameters Δ_{pf} and t, together with invariant t', *i.e.* a given renormalized band-structure is to be assumed and then connected by MFSB equations to bare values of parameters Δ_{pd} and t_0. This does not lead necessarily to apparent contradictions even if inadequate renormalized band regime is chosen for given bare values Δ_{pd}, t_0 and t'.

The first step is therefore to discuss the renormalized three-band structure in whole Δ_{pf}, t, t' parameter-space and to determine qualitatively which regions of this space correspond to strong renormalization. Once this is accomplished, the renormalized band-structures are to be used in MFSB equations to determine the associated bare values of Δ_{pd}, t_0 and t'.

The second step is to deal with integral nature of the MFSB equations. This can be done by inverting the usual order of the operations into integration over $\mathbf{k}$ first and the differentiation later, $\mathbf{k}$ integration performed to the leading order of t'. The results are three coupled algebraic rather than the integral MFSB equations.

This procedure is carried out here. It generates the analytical expressions which answer all basic questions mentioned above, together with a number of other results. In particular, the experimentally measured band-structure with their doping dependencies can be compared to the renormalized MFSB results in the whole parameter space. Prerequisite to such comparison is the knowledge of the propagators for physical particles. This problem is discussed in the companion paper [23], arguing that the MFSB renormalized dispersion appears as a resonant band of the physical single-particle spectrum. The physical spectrum is shown there to obey the Luttinger sum rule, which is important for positioning the Fermi surface, the property best seen in the angle-resolved photoemission spectroscopy (ARPES) experiments [24–28].

In Section 2, the MFSB approach to the $U_d = \infty$ Emery model is thus briefly reviewed. Section 3 is devoted to the description and discussion of the possible three-band structures, which, as more or less renormalized, enter the MFSB equations. In Section 4 the MFSB equations are derived in the algebraic form and solved analytically in the appropriate limits. Section 5 compares the predictions of the $U_d = \infty$ MFSB theory with the experimental results. Finally, Conclusion summarizes the new results obtained here and enumerates the remaining open questions.

2 MFSB approach - General

In this section $U_d = \infty$ MFSB formulation [12,16,23] is briefly reviewed, with the emphasis on the aspects important for the present approach. The free part h_0 of the Emery Hamiltonian is

$$h_0 = \sum_{s,R}\{\varepsilon_d n_R^d + \varepsilon_p \sum_{i=x,y} n_{R,i}^p + \sum_{i=x,y}[t_0 c_{R,s}^\dagger (p_{R,i,s} + \sum_r t_0(r) p_{R+r,i,s} + \text{h.c.})] - t'[p_{R,x,s}^\dagger (p_{R,y,s} + \sum_r t'(r) p_{R+r,y,s} + \text{h.c.})]\}, \quad (1)$$

where $c_R^\dagger$ creates a hole on the Cu site and $p_{R,i}^\dagger$ creates it on the O site, R is site index, s is spin index and r runs over the nearest neighbors. Here we use the usual, non-magnetic, undistorted CuO_2 square unit cell with $d_{x^2-y^2}$ ionic wave functions associated with the Cu site, whereas the oxygen sites on the x and y axes are associated with the p_x and p_y states, respectively. The phases of the involved states, *i.e.* the signs of $t_0(r)$ and $t'(r)$ are chosen in usual way [13,29]. When the local interaction U_d on the Cu sites $U_d \sum_R n_{R,\uparrow}^d n_{R,\downarrow}^d$ is taken to infinity with respect to $\Delta_{pd} = \varepsilon_p - \varepsilon_d$, the splitting of O and Cu site energies, the physical d-fermion operator $c_R^\dagger$ is conveniently represented by a two particle entity $f_R^\dagger b_R$ composed of the f-fermion and the b-boson. Double occupancy is forbidden by the requirement

$$Q_R = n_R^f + b_R^\dagger b_R = 1 \quad (2)$$

taken into account through the Lagrange multipliers λ_R in

$$H = h_0 + \sum \lambda_R (Q_R - 1) \quad (3)$$

i.e. allowing the fluctuations in Q_R. In this case, the relation between n_R^d and n_R^f has to be specified, in particular for the representation of the ε_d term of h_0 in equation (1). The usual choice [7] is

$$n_R^d = n_R^f \quad (4)$$

extending this equality from $Q_R = 1$ subspace to the whole boson-fermion Hilbert space.

The usual [23] MFSB procedure approximates the ground state of H by the product of the boson and spin unpolarized fermion states. Taking $\lambda_R = \lambda$ in equation (3) and allowing for $\langle b_R^\dagger \rangle = \langle b_R \rangle = b_0$, the approximate ground state energy of H, given by equations (3) and (4) is

$$E = E_0 + (\Delta_{pd} - \Delta_{pf})\left(\frac{t^2}{t_0^2} - 1\right), \quad (5)$$

where $\Delta_{pf} = \varepsilon_p - \varepsilon_d + \lambda = \Delta_{pd} + \lambda$ and $t = t_0 b_0$. E_0 is the ground state energy of free auxiliary fermions, described by the non-interacting Emery Hamiltonian (1), with the replacement $c_R^\dagger$ by $f_R^\dagger$, ε_d by $\varepsilon_f = \varepsilon_d + \lambda$ and t_0 by t, ε_p and t' being unchanged. E_0 is thus given by

$$E_0(\Delta_{pf}, t, t', x) = \int^\mu \varepsilon g(\varepsilon) \mathrm{d}\varepsilon, \quad (6)$$

where $g(\varepsilon)$ is the density of states of the three-band Emery model. Since b_0 and λ, *i.e.* t and Δ_{pf}, are to be determined from the minimization of E of equation (5) at fixed number of particles, $1+\delta = \langle n^f \rangle + 2\langle n^p \rangle$, (using again Eq. (4)), additional equation relating δ and μ is required,

$$1 + \delta = \int^\mu g(\varepsilon) \mathrm{d}\varepsilon. \quad (7)$$

Minimizing equation (5) with respect to Δ_{pf} gives [16,23,30]

$$\langle n^d \rangle + t^2/t_0^2 = 1 \quad (8)$$

with

$$\langle n^d \rangle = -\frac{\partial E_0}{\partial \Delta_{pf}} \quad (9)$$

according to equation (4). Clearly, equation (8) forbids double occupation of the Cu site only at average, $\langle n^d \rangle \leq 1$. The minimization of E with respect to t gives [16,23,30] the second MFSB equation

$$\langle n^B \rangle = 2\frac{t(\Delta_{pd} - \Delta_{pf})}{t_0^2} \quad (10)$$

with

$$\langle n^B \rangle = -\frac{\partial E_0}{\partial t}, \quad (11)$$

$\langle n^B \rangle$ denoting the renormalized Cu-O bond-charge. Noteworthy, $\langle n^B \rangle$ vanishes at $t = 0$, corresponding to the Mott localization of the f-fermions.

While equations (5–9) determine the approximate ground state energy and the corresponding average charge distribution $\langle n^d \rangle$ and $\langle n^p \rangle$, a step further is required [23] to find the propagator of the physical particles, important for the comparison to other experiments, ARPES in particular.

This step, described in detail in the companion paper [23], consists of including the fluctuations of auxiliary fields around their saddle point values on neglecting their interaction. For the propagator of the physical fermion between Cu-sites this results [23] in the resonant band and the dispersionless background structure

$$G^d(\omega, \mathbf{k}) = (1 - \langle n^d \rangle) G^f(\omega, \mathbf{k}) + \langle n^d \rangle \int \frac{\mathrm{d}\mathbf{k}}{(2\pi)^2} \hat{G_c^f}(\omega + \Delta_{pd} - \Delta_{pf}, \mathbf{k}) \quad (12)$$

where G^f is the f-fermion propagator. Its projection $\hat{G^f}$ on the occupied states of the conduction band,

$$\hat{G_c^f}(\omega, \mathbf{k}) = \frac{|m_f^c(\mathbf{k})|^2 \theta(\mu - \varepsilon_c(\mathbf{k}))}{\omega - \varepsilon_c(\mathbf{k}) - \mathrm{i}\eta}, \quad (13)$$

contains f-fermion MFSB renormalized dispersion $\varepsilon_c(\mathbf{k})$ of the f-fermion conducting band (assuming single for

simplicity) and $|m_f^c(\mathbf{k})|^2$ describes the projection of the corresponding $\mathbf{k}$ state on the Cu-site. As clear form equations (12, 13), the position of the resonant band is associated with ε_f and that of the dispersionless background with ε_d. It is appropriate to mention here that MFSB theory neglects the "lifetime" effects (present in the treatment beyond it, such as non-crossing approximation (NCA) [31] or dynamical mean field theory (DMFT) [10]), emphasizing spatial dispersions, *i.e.* the $\mathbf{k}$ dependencies. In addition, equations (12–13) should not be used for too small δ, although they give approximately the site energy ε_f of the t-J singlet, unlike its dispersion, dominated by magnetic correlations.

The propagator (12) satisfies [23] the Luttinger sum rule: with μ calculated from the MFSB equation (7) for f-fermions the number of d-holes on the Cu-site in the resonant band is $(1-\langle n^d\rangle)\langle n^d\rangle$, while in the background it is $\langle n^d\rangle^2$, altogether this makes $\langle n^d\rangle$ of equations (4–8). In other words, the Fermi surface in the MF f-fermion conduction band $\varepsilon_c(\mathbf{k})$ encloses through equations (4–8) just as many f-particles as the Fermi surface of the same shape of the resonant band of equation (12), contribution of the background added of the physical d-particles; the Fermi surface calculated in the MFSB theory, equation (7), is observable as the physical Fermi surface in the resonant band. This conclusion is crucial for the comparison of the present theory with ARPES experiments.

Equations (7, 8, 10) which determine the physical propagator $G^d(\omega,\mathbf{k})$ of equation (12) in the reciprocal space, including the local property $\langle n^d\rangle$, represent a set of coupled integral equations. For a given renormalized band structure characterized by Δ_{pf}, t, t', this set of equations determines the corresponding bare parameters Δ_{pd} and t_0 for a chosen δ. The inversion of these equations is thus required to find Δ_{pf} and t as functions of bare parameters Δ_{pd}, t_0, t' at given δ.

In its full generality, this is a difficult problem. The numerical procedures [13,19–21] usually assume the form of the renormalized 3-band solution, *i.e.* choose the regimes for Δ_{pf}, t, t' and solve the MFSB equations to find the corresponding Δ_{pd} and t_0. This is usually restricted to a small number of points in the Δ_{pf}, t, t' parameter space. Related and already mentioned difficulty arises from the fact that when a given Δ_{pf}, t, t' is inserted into equations (8–11), it "produces" a set of Δ_{pd} and t_0 with no apparent contradictions when the latter actually correspond to a different regime of Δ_{pf}, t, t'.

It is thus obviously important to distinguish first between all the regimes of Δ_{pf}, t, t' 3-band model and to determine qualitatively the corresponding regimes of bare parameters Δ_{pd}, t_0 and t'. Using in the next step the appropriate expressions for the renormalized band-structure, the MFSB equations (7)-(11) are to be inverted in order to find Δ_{pf}, t as functions of Δ_{pd}, t_0 t' and δ. This procedure is carried out here analytically, assuming $\mathrm{sign}t' = -\mathrm{sign}\Delta_{pf}$ and δ small for arbitrary Δ_{pd}/t_0, t'/t_0, interesting for high-T_c superconductors.

3 Three band-structure

The first step consists thus of the discussion of the three band-structure of the effectively free Emery model (1) characterized by Δ_{pf}, t and t'. The Bloch states are built in the usual tight-binding way from $d_{x^2-y^2}$, p_x and p_y states in each unit cell and the effective band-energies $\varepsilon_i(\mathbf{k})$ are found by diagonalization of the corresponding 3×3 Hermitian matrix.

This diagonalization leads to the secular equation of the third order

$$\varepsilon^3 + 3p\varepsilon + 2q = 0, \tag{14}$$

where

$$\begin{aligned} p &= -[\alpha + \beta f_1(\mathbf{k}) + \gamma f_2(\mathbf{k}),\\ q &= a + b f_1(\mathbf{k}) + c f_2(\mathbf{k})\,, \end{aligned} \tag{15}$$

with

$$\begin{aligned} &a = \frac{1}{27}\Delta_{pf}^3,\ b = \frac{2}{3}t^2\Delta_{pf},\ c = -\frac{16}{3}t'[t'\Delta_{pf} + 3t^2],\\ &\alpha = \frac{1}{9}\Delta_{pf}^2,\ \beta = \frac{4}{3}t^2,\ \gamma = \frac{16}{3}t'^2\,, \end{aligned} \tag{16}$$

and

$$\begin{aligned} f_1(\mathbf{k}) &= \sin^2\frac{k_x}{2} + \sin^2\frac{k_y}{2},\\ f_2(\mathbf{k}) &= \sin^2\frac{k_x}{2}\sin^2\frac{k_y}{2}. \end{aligned} \tag{17}$$

Energy ε is measured with respect to $\widetilde{\varepsilon} = (2\varepsilon_p + \varepsilon_f)/3$. The dispersion f_1 is associated in equations (16) and (17) with Cu-O hopping t and describes propagation along the main axes of CuO_2 unit cell while f_2 is related to O-O hopping t', denoting the propagation along the diagonals. The rotation of the Fermi surface by $\pi/4$ observed in LSCO corresponds then here, quite generally, to the transition from the dominant O-O hopping t' to the dominant effective Cu-O hopping t.

It should be noted further that equation (14) is invariant on the simultaneous change of sign $\Delta_{pf}, t', \varepsilon$ irrespectively of the sign of t. This parametric symmetry means that the band structure $\varepsilon_i(\mathbf{k})$ for $\mathrm{sign}\Delta_{pf} = \mathrm{sign}t' < 0$ or $\mathrm{sign}\Delta_{pf} = -\mathrm{sign}t' < 0$ can be obtained from the $\varepsilon_i(\mathbf{k})$ for $\mathrm{sign}\Delta_{pf} = \mathrm{sign}t' > 0$ or $\mathrm{sign}\Delta_{pf} = -\mathrm{sign}t' > 0$ respectively by the reflection on the $\mathbf{k}$ plane. We shall therefore, without the loss of generality, carry out the theoretical discussion for $t, \Delta_{pf} > 0$ and for both signs of t'.

It can be finally noted that the band structure in the electron language, usual in the ARPES analysis is obtained from the band structure in the hole language used here also by the reflection on the $\mathbf{k}$ plane.

3.1 Small t

At the outset it is instructive to start to consider the limit of small t, because all of the conceptually important properties of the 3-band structure occur already in this limit

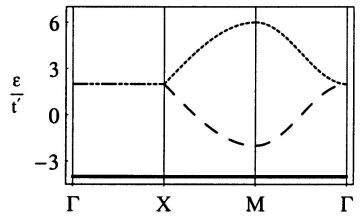

Fig. 1. $t = 0$ band-structure.

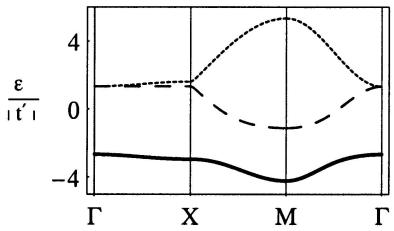

Fig. 2. Anticrossing of two lower bands for $\Delta_{pf}/t' = -4$ and $t/t' = -0.3$.

on the simple perturbative level. Moreover, this limit will turn out here as central to the MFSB theory of the high-T_c superconductors, although the opposite limit of small t' (or even $t' = 0$) [7] was usually used in this context.

The $t = 0$ band structure of equation (14) is given by dispersionless copper level

$$\varepsilon_L^{(0)}(\mathbf{k}) = -\frac{2}{3}\Delta_{pf} \tag{18}$$

and by two oxygen bands

$$\varepsilon_{I,U}^{(0)}(\mathbf{k}) = \frac{1}{3}\Delta_{pf} \pm 4|t'|f_2. \tag{19}$$

and shown in Figure 1 for $\Delta_{pf} > 4|t'|$.

As apparent from equation (19), oxygen two band structure unfolds into a single oxygen band in the $\sqrt{2}$ Brillouin zone, which corresponds to the $1/\sqrt{2}$ unit cell containing one oxygen, as appropriate for oxygens when they are decoupled from copper. This means in particular that the degeneracy of two oxygen bands of equation (19) along ΓX line in Figure 1 corresponds to the two-dimensional logarithmic vH singularity in the density of states rather than to the extended one-dimensional one: the energy varies linearly with $\mathbf{k}$ through ΓX line.

Introducing further small t and considering energies ε close to $\varepsilon_L^{(0)}$ on assuming that $\varepsilon_U^{(0)}$ is far from $\varepsilon_L^{(0)}$, the iterative solution of equation (14) is given by quadratic, rather than cubic equation

$$(\varepsilon - \varepsilon_L^{(0)})(\varepsilon - \varepsilon_I^{(0)}) = -\frac{2t^2(3f_1\varepsilon + 16t'f_2)}{\varepsilon_L^{(0)} - \varepsilon_U^{(0)}}, \tag{20}$$

valid for $\Delta_{pf} \approx 4|t'|$ or $\Delta_{pf} > 4|t'|$. Equation (20) is characteristic for band anticrossing, familiar from Wigner perturbation theory, to which it is essentially equivalent. Characteristic anticrossing situation is shown in Figure 2. Simplifying for clarity, anticrossing occurs when $\varepsilon_L^{(0)}$ is chosen equal to $\varepsilon_I^{(0)}$ in equation (20), but the finite value of the numerator on r.h.s. of this equation makes ε_L differ from ε_I. Indeed, for sign $\Delta_{pf} = -\text{sign}t'$, the numerator is finite, noting that, for that purpose, ε in it can be replaced by $\varepsilon_L^{(0)}$ of equation (18). However, this numerator can vanish for $\text{sign}\Delta_{pf} = \text{sign}t'$. *E.g.* for band-crossing in **M** point of BZ $f_1 = 2, f_2 = 1$, $\varepsilon_I^{(0)} = \Delta_{pf}/3 - 4|t'| = \varepsilon_L^{(0)}$, the numerator vanishes exactly and two bands touch each other $\varepsilon_L = \varepsilon_I = \varepsilon_L^{(0)} = \varepsilon_I^{(0)}$. As suggested earlier, touching persists for sign $\Delta_{pf} = \text{sign}t'$, when Cu-level $\varepsilon_L^{(0)}$ enters into the oxygen $\varepsilon_I^{(0)}$ band, as it will be further discussed below, for the cubic equation (14). There, it will be also shown here that in addition to the original suggestion [29], touching can occur for $\text{sign}\Delta_{pf} = -\text{sign}t'$, but at sufficiently large t.

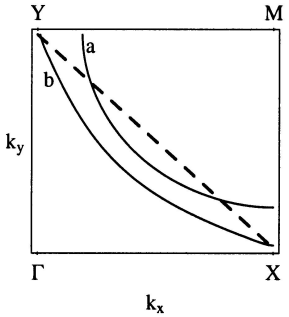

Fig. 3. Equienergetic contours of ε_L obtained for $\Delta_{pf} > 0$ and small $t' \leq 0$; (a) – energy ε_0 that separates the number of states below and above it in two halves, (b) – equienergetic curve ε_{vH} that passes through van Hove points, dashed line – equienergetic line at $t' = 0$ that passes through van Hove points at ε_{vH}.

Before going to this discussion, equation (20) can be used to illustrate an important topological property of the lowest band, also related to the relative sign of Δ_{pf} and t'. This can be best seen on simplifying further equation (20) by assuming that $\varepsilon_L^{(0)}$ is far from both $\varepsilon_{U,I}^{(0)}$. Wigner equation (20) reduces then to the Schrödinger perturbative expression

$$\varepsilon - \varepsilon_L^{(0)} = -\frac{4t^2(\Delta_{pf}f_1 - 8t'f_2)}{\Delta_{pf}^2 - 16t'^2f_2^2}, \tag{21}$$

valid for $\Delta_{pf} > 4|t'|, t$. It appears from equation (21) that while t determines the overall scale for the dispersion of the band $\varepsilon_L(\mathbf{k})$, t' measures itself with respect to Δ_{pf}, independently on t: t' can be treated as small for $|t'| < \Delta_{pf}$.

For t' small, the equienergetic line $\varepsilon_L(\mathbf{k}) = \varepsilon_{vH}$ through the **X** point of BZ is bent towards **Γ** point for $\text{sign}\Delta_{pf} = -\text{sign}t'$, as shown in Figure 3, or towards **M** point, if $\text{sign}\Delta_{pf} = \text{sign}t'$.

The same conclusion applies to ε_U, which becomes the lowest band ε_c by parametric symmetry of equation (14), when $\Delta_{pf} < 0$. Fermi surfaces measured in high-T_c materials are bent towards **Γ** point, indicating $\text{sign}\Delta_{pf} = -\text{sign}t'$. As this can occur either in ε_L for $\Delta_{pf} > 0, t' < 0$ or in ε_U for $\Delta_{pf} < 0, t' > 0$, the

absolute sign of Δ_{pf} or t' cannot be determined from Fermi surface topology.

As discussed above, the relative sign of Δ_{pf} and t' defines also the anticrossing/touching properties of the 3-band structure. The following subsection is therefore dedicated to the analysis of the latter property.

3.2 Band degeneracy

In the analogy with the general condition for the band-touching in equation (21) which is the vanishing of the discriminant of the quadratic equation, the general condition for the band-touching in the full cubic equation (14) is the vanishing of its discriminant, *i.e.*

$$D = q^2 + p^3 = 0 \tag{22}$$

with p and q given by equations (15–17). For $D = 0$ with $p^3 = -q^2 \neq 0$, two roots of the cubic equation are degenerate and different from the third one. The hermiticity of the 3×3 matrix underlying equation (14), ensures that $D \leq 0$, *i.e.* that all the roots are real. This means that the zero of D at a given point $\mathbf{k}$ of the BZ is also the maximum of D, which can be conveniently associated [15,16] with

$$\frac{\partial D}{\partial f_1} = 0 \tag{23}$$

and

$$\frac{\partial D}{\partial f_2} = 0. \tag{24}$$

The system of three equations (22–24) for two unknowns k_x and k_y is overdefined and thereby does not posses a solution for general values of the two parameters involved, *e.g.* t/t' and Δ_{pf}/t'. Nevertheless,there exists a whole region in this (two)-parameter space, where three equations (22), (23) and (24) can be satisfied simultaneously.

Equations (23–24) allow to separate out the trivial $f_1 = 0$ degeneracy of two oxygen bands in $\mathbf{\Gamma}$ point, which occurs irrespectively on the values of parameters. This lowers the degree of coupled equations in f_1. It becomes also apparent that equation (24) is satisfied for symmetry reasons on $\mathbf{\Gamma X}$ and $\mathbf{\Gamma M}$ axes of BZ, irrespectively on the value of f_1. It is then possible to show analytically [15,16] that Δ_{pf}/t' and t/t' can be tuned to bring the solution of the two other equations to the high-symmetry axis, specifically to $k_x = k_y$ $\mathbf{\Gamma M}$ line, and to determine the range of parameters for which this can occur. For $\mathrm{sign}\Delta_{pf} = \mathrm{sign}t'$, it has already been shown above that at small t for $\Delta_{pf} = 4t'$, the touching occurs for $f_1 = 2$, *i.e.* at $\mathbf{M}$ point of BZ. For $0 < \Delta_{pf}/t' < 4$, it occurs at

$$2f_1 = \frac{\Delta_{pf}}{t'} + \frac{t^2}{t'^2} \tag{25}$$

on the isolated point on $\mathbf{\Gamma M}$ line. When t^2/t'^2 increases,the touching point moves from $t \approx 0$, $4f_2t' \approx \Delta_{pf}$ (Fig. 1) towards $\mathbf{M}$ point (Fig. 4a), which is reached (Fig. 4b) for $f_1 = 2$ in equation (25).

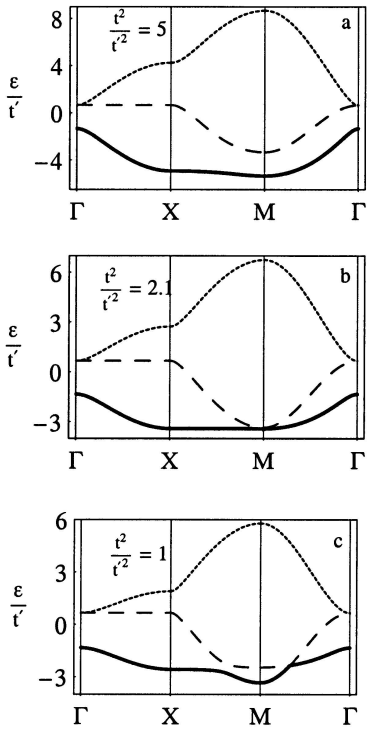

Fig. 4. Three-band structure for $\Delta_{pf} > 0$: $\Delta_{pf}/t' = 2$: at t^2 large, ε_L and ε_I are well separated (a), at critical value of t^2/t'^2, given by equation (25), they touch at the $\mathbf{M}$ point of the BZ (b), for smaller values of t^2/t'^2, the touching point moves down the zone-diagonal towards $\mathbf{\Gamma}$ (c).

Figure 4c illustrates the situation for even larger t^2/t'^2. For $\mathrm{sign}\Delta_{pf} = -\mathrm{sign}\,t'$, the anticrossing found above for small t, with ε_I bent towards ε_L on $\mathbf{M}$ point (Fig. 2), spreads for large t all over the BZ. Finally, as shown on Figure 5, ε_L and ε_I are repelled even in $\mathbf{M}$ point and ε_I becomes flat [16], (somewhat unexpectedly all over the BZ, as it is for $t' = 0$) for

$$\frac{t^2}{t'^2} = -\frac{\Delta_{pf}}{2t'}\cdot \tag{26}$$

This corresponds to the appearance of the double zero in D at $f_1 = 0$, *i.e.* to the touching of ε_U and ε_I in $\mathbf{\Gamma}$.

For even larger values of t/t', ε_I bends towards ε_U (Fig. 5b) and the touching moves from $\mathbf{\Gamma}$ towards $\mathbf{M}$ for $t^2/t'^2 > -\Delta_{pf}/2t'$. Finally, for $f_1 = 2$ in equation (25), the touching of ε_I and ε_U reaches $\mathbf{M}$ point (Fig. 5c). For even larger values of t^2/t'^2, a perturbative regime with respect to small t' is reached (Fig. 5d), similar to the one for $\Delta_{pf} \gg 4t'$ when $\mathrm{sign}\Delta_{pf} = \mathrm{sign}t'$ (Fig. 4c).

The results of the present analysis are summarized in Figure 6. which associates different regimes of the 3-band structure with the corresponding parts of Δ_{pf}/t', t/t' parameter space.

Noteworthy in this figure is that the $\mathbf{M}$ touching line $f_1 = 2$ of equation (25) is continuous through the $\Delta_{pf}/t' = 0$ point. In the presentation adopted here, with $\Delta_{pf} > 0$, this corresponds to t' varying from + to − infinity and, respectively, the touching from $\varepsilon_I/\varepsilon_L$ to

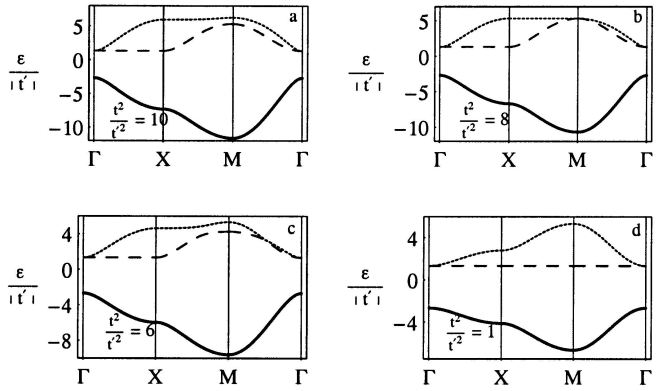

Fig. 5. Three-band structure for $\Delta_{pf} > 0$: $\Delta_{pf}/t' = -4$: at t^2/t'^2 large, ε_U and ε_I are degenerate only in **Γ** point (a), at critical value of t^2/t'^2, given by equation (25), they touch at the **M** point (b), for smaller values of t^2/t'^2, the touching point moves down the zone-diagonal towards **Γ** point(c), at t^2/t'^2 given by equation (26), ε_I becomes flat (d).

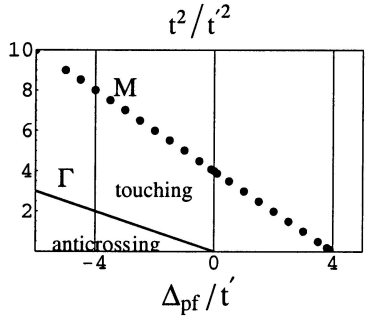

Fig. 6. Different kinds of three-band topology depending on the values of the effective parameters, with $\Delta_{pf} > 0$: for $t' > 0$ and $\Delta_{pf}/4t' > 1$, ε_L and ε_I are separated (bar), for a critical value of t^2/t'^2, touching between two lower ($t' > 0$) or upper ($t' < 0$) bands occurs at the **M** point (dots), region of band-touching is limited with the condition (26) (line) and evolves into the anticrossing behavior of two lower bands.

$\varepsilon_I/\varepsilon_U$. The continuity, not obvious in this way, becomes clear if Figure 6 is read using the parametric symmetry of equation (25), as corresponding to the change of sign Δ_{pf} at fixed $t' > 0$ (Fig. 5 should be used then with $\varepsilon \to -\varepsilon$). The touching then occurs always in the lowest band towards which ε_I bends for $t' > 0$ whatever is the sign of Δ_{pf}. A somewhat larger value of t' is then required, continuously at $\Delta_{pf} = 0$, for ε_I to cross the gap Δ_{pf} to ε_L for $\Delta_{pf} > 0$ than for $\Delta_{pf} < 0$ when the gap to ε_U ceases to exist.

3.3 Extended van Hove singularities

Touching of two bands at **M** point is interesting from another respect. From Figures 4 and 5, it can be seen that the above touching is accompanied by the absence of the dispersion on the **XM** line, either in ε_L or in ε_U band. This leads to the coalescence of the step-like vH singularity [24] at the bottom of the band (**M** point) and the logarithmic singularity at **X** point in the density of states, resulting in the extended, 1-d-like singularity. The extended vH singularity can thus occur in 3-band model, (only) when the Fermi energy for one hole per CuO_2 cell intersects two bands close to the **M** point, as illustrated in Figure 7.

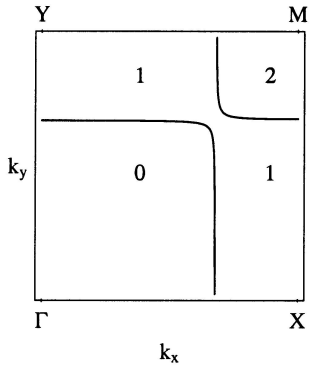

Fig. 7. Typical shape of the Fermi surfaces when band-touching takes place.

This situation has never been observed in high-T_c cuprates.

4 MFSB equations at finite t′

4.1 Qualitative MFSB analysis

This section begins with several observations concerning MFSB aspects of different regimes of Figure 6. The observations in question are based on equation (9) of the MFSB theory, which requires $\langle n_d \rangle \leq 1$ in such a way that $\langle n_d \rangle = 1$ corresponds to $t = 0$. With one hole per unit cell, $\langle n \rangle = 1$ and for any $\Delta_{pf} < 4|t'|$ the holes are necessarily transferred from Cu to O resulting in $\langle n_d \rangle < 1$, *i.e.* $t > 0$ regime. Critically renormalized $t = 0$ regime can thus be (but not necessarily) stable only for $\Delta_{pf} > 4|t'|$. Considering Figure 6, this corresponds to $\Delta_{pf}/t' > 4$ when $t' > 0$ and $\Delta_{pf}/t' < -4$ when $t' < 0$.

Critically renormalized regime $t = 0$ at $n = 1$ ($\delta = 0$) depends also critically on doping. This can be easily understood on invoking again MFSB equation (8) for $\Delta_{pf} > 4|t'|$, allowing $t = 0$ for $\langle n_d \rangle = 1$, but not allowing it for $n = 1 + \delta$, with $\delta > 0$, which, at $t = 0$, leads to forbidden $\langle n_d \rangle = 1 + \delta$.

The stability of $t = 0$ solution at $\delta = 0$, *i.e.* the BR phase transition can be examined using equation (20) for renormalized band-structure in MFSB equations. Actually, the simplified version (21) of equation (20) is sufficient for $t = 0$ small. Since the regime $\Delta_{pf} > 4t'$ for $t' > 0$ is ruled out for high-T_c superconductors by the condition $\mathrm{sign}\Delta_{pf} = -\mathrm{sign}t'$ obtained from the topology of the observed FS, the attention here will be focused on the stability of $t = 0$ solution in the anticrossing case $\Delta_{pf} > -4t'$ for $t' < 0$.

Noncritical renormalization $t > 0$ at $\delta = 0$, for $\Delta_{pf} < 4|t'|$ will also be considered in order to complete

well-known $t' = 0$ MFSB result with the illustration how (fast) weakly renormalized regime $\Delta_{pf} \approx \Delta_{pd}$ and $t \approx t_0$ is reached in this case.

4.2 Conducting band at the limit of small t′

It is convenient to start the quantitative discussion with the limit $\Delta_{pf} > 4|t'|$ when t' term in the denominator of equation (21) can be neglected. Actually, in the limit of t' small, equation (21) can be replaced by more general expression

$$\varepsilon_L = -\frac{1}{2}\left[\Delta_{pf} + \sqrt{\Delta_{pf}^2 + 16t^2 f_1}\right] + \frac{32t^2 t' f_2}{\Delta_{pf}^2}, \qquad (27)$$

which, with $|t'|$ small makes no assumption concerning the relative values of Δ_{pf} and t. For small t, equation (27) reduces to equation (21), except that the energy-origin at $(\varepsilon_f + 2\varepsilon_p)/3 = 0$ in equation (21) is shifted to $\varepsilon_p = 0$ in equation (27), as appropriate for MFSB calculations, which, in contrast to ε_f, do not renormalize ε_p. Equation (27) does not only determine the MFSB stability for $t = 0$, but also for arbitrary t, linearly in t'.

Figure 2 used to illustrate the behavior of ε_L of equation (21) for small t' applies also to equation (27), because $\varepsilon = \varepsilon_{vH}$ equienergetic line through the van Hove (vH) points coincides with the diagonal for arbitrary t and is deformed with t' in the indicated way. When MFSB equations are considered with the band ε_L of Figure 2, it is seen that they require the integration of the constant (Eq. (7)) or of ε_L itself (Eq. (6)) up to the Fermi energy μ. These integrations can be carried out analytically, with controlled accuracy in t', by decomposing the integration over $\mathbf{k}$ in three steps. In the first step the integration goes from the $\mathbf{M}$ point to the diagonal in Figure 3. In the second step the integration covers the range between the diagonal and the equienergetic ε_{vH} line. The departure of ε_L from the diagonal is then taken linear in t'. In the third step, the integration is carried out between two equienergetic lines ε_{vH} and μ with the departure of ε_L from the diagonal linearized in t'.

When the procedure is applied to equation (7) for the number of particles, the total number of states δ_c introduced by $t' < 0$ below ε_{vH} is found, as well as the number of states between two close energies ε_L. For $\Delta_{pf} > |t'|$, in the corresponding limit of equation (21), this gives

$$\delta_c = -\frac{32t'}{\pi^2 \Delta_{pf}}, \qquad (28)$$

the position of the Fermi level μ for a given δ, $\Delta_{pf}(\varepsilon_{vH} - \mu) = 16t^2\kappa_F$

$$\left(1 + \frac{\pi^2\delta_c}{8}\right)\kappa_F \ln\frac{1}{|\kappa_F|} = 8\pi^2(\delta_c - \delta), \qquad (29)$$

and, by the differentiation of equation (29) with respect to δ, the density of states at the energy μ close below (or above) ε_{vH}

$$n_L(\mu) = \frac{2\Delta_{pf}}{\pi^2 t^2}\left(1 + \frac{\pi^2\delta_c}{8}\right)\ln\frac{1}{|\kappa_F|}. \qquad (30)$$

Equations (28) and (29) show that the Fermi level of a half-filled ($\delta = 0$) band is removed from vH singularities. δ_c is the doping required at finite t' to bring it back, and that doping is, just like the corresponding κ_F at given δ, independent on t. The latter property is a consequence of already noted fact that the overall dispersion scale in equations (20, 21) or (27) is given by t^2, *i.e.* that t' affects ε_L only when t is finite.

Equation (30) can also be obtained by expanding the closed expression for the density of states available [15,16,32] in $\Delta_{pf} > t$ limit of equation (27), in the neighborhood of vH singularity. The advantage of equations (28–30) is however that they describe the effects of δ_c and δ small only in terms of the states in the vicinity of the vH energy, deeper, always filled states thus removed from the problem.

Expressions analogous to equations (28–30) are obtained from equation (27) for $t > \Delta_{pf}$; essentially, Δ_{pf} in equations (28–30) is replaced by t [23]. However, they are of lesser interest here and we turn to the determination on the MFSB energy E_0 for $\Delta_{pf} > t$, adding from equation (27) a term quartic in t to equation (21), with t' neglected in its denominator.

4.3 Inversion of MFSB equations at small t′

While equations (28–30) can be in principle also obtained by the expansion of the closed expression for the density of states there exists no such expression for the energy E_0 of equations (6) and (27).

Three-steps procedure introduced here provides then the expansion of E_0 from the outset with the same accuracy as equations (28–30). Using the described integration procedure, E_0 is straightforwardly found as

$$E_0 = -\Delta_{pf}(1+\delta) + \frac{\mu - \varepsilon_{vH}}{2}(\delta_c - \delta) - \frac{4t^2}{\Delta_{pf}}(c_1 + \delta_c c_3 + \delta) + \frac{16t^4}{\Delta_{pf}^3}c_2 \qquad (31)$$

retaining the term quartic in t. Here $\mathbf{k}$-integration constants c_i are given by

$$c_1 = 1.405, c_2 = 2.06, c_3 = 2.07. \qquad (32)$$

Consistently with equation (27), the terms quadratic in δ_c are omitted from equation (31). The $(\mu - \varepsilon_{vH})\delta_c \sim \kappa_F\delta_c$ term, which is according to equation (29) even smaller than the omitted δ_c^2 terms is however retained, because it is the first term of the logarithmic nature, generated by equation (27). The logarithmic signature κ_F of the 2d vH singularity (30) appears explicitly in this term, which is on the other hand clearly related by equation (29) to breaking at $\delta = 0$ of the local, conduction band electron-hole symmetry with respect to the vH singularity. The definition of κ_F in equation (29) shows however that this term is proportional to t^2/Δ_{pf}, *i.e.* that it can be merged with the third term in equation (31). These terms vanish at $t = 0$, *i.e.* neither δ_c, nor $\kappa_F\delta_c$ can suppress

the BR transition to the $t = 0$ state, contrary to what is suggested by equation (29) itself, where δ_c appears as the effective doping.

Although δ_c and $\kappa_F\delta_c$ do not suppress the BR transition, they shift its position, change its nature and modify the behavior far from the transition point. The role of δ_c and $\kappa_F\delta_c$ can now be discussed using equation (31) in MFSB equations to obtain

$$\langle n_d\rangle = 1+\delta-\frac{4t^2}{\Delta_{pf}^2}\Bigg[c_1+2\delta_c c_3+6\kappa_F\delta_c+(1-2\kappa_F)\delta - \frac{12t^2}{\Delta_{pf}^2}c_2\Bigg] = 1-\frac{t^2}{t_0^2} \quad (33)$$

and

$$\langle n_B\rangle = -\frac{8t}{\Delta_{pf}}\Bigg[c_1+\delta_c c_3+2\kappa_F\delta_c+(1-2\kappa_F)\delta - \frac{8t^2}{\Delta_{pf}^2}c_2\Bigg] = \frac{2t}{t_0^2}(\Delta_{pd}-\Delta_{pf}). \quad (34)$$

It should be emphasized once again that the main simplification in the derivation of these equations corresponds to the use of three-step $\mathbf{k}$ integration procedure to find E and μ, (*i.e.* κ_F) before taking slave-boson derivatives, rather than taking these derivatives before $\mathbf{k}$ integration, as usual in the conventional theory. Also, in contrast to the conventional theory, where the grand-canonical potential $\Omega = E-\mu(1+\delta)$ is usually used to perform MFSB derivatives with respect to Δ_{pf} and t at constant μ, at $t' \neq 0$ it is simpler to use E_0 of equation (31) to find the derivatives at constant δ. In particular, as already explained below equation (29) κ_F does not depend on t at constant δ.

Equation (29) and second equalities (33) and (34) invert analytically three MFSB coupled integral equations, which express Δ_{pd} and t_0 as functions of Δ_{pf}, t, t', μ into (only two, when κ_F can be omitted) algebraic equations, which solve for Δ_{pf} and t as functions of Δ_{pd}, t_0 and δ, linearized in t'. These solutions are considered next.

4.4 Vicinity of BR transition, $\Delta_{pd} \approx \Delta_{pd}^{cr}$ at small t′

In order to describe the effect of δ_c and $\kappa_F\delta_c$ on the position and the nature of the BR transition in the spirit of the perturbative treatment of t', it is convenient to expand equations (33) and (34) around $t' = 0$ BR critical point. As well known, and also easily seen from equation (33) and (34), the latter occurs at $\Delta_{pd} = \Delta_{pd}^{cr}(t' = 0) = 4.74t_0\sqrt{c_1}$ with $\Delta_{pf} = \Delta_{pf}^{cr}(t'=0) = \Delta_{pd}^{cr}/2$. Setting thus

$$\Delta_{pd} = \Delta_{pd}^{cr}(1+\eta), \quad (35)$$

$$2\Delta_{pf} = \Delta_{pd}^{cr}(1+2\eta+\epsilon), \quad (36)$$

and assuming ϵ, η small, equation (34) becomes

$$2c_1^2t^2 = c_2t_0^2(\epsilon^2-2\eta+a_2) \quad (37)$$

to the leading order in ϵ, η, and t/t_0. Noteworthy, the term linear in ϵ cancels out in equation (37), making ϵ^2 term important. Inserting equation (37) in the expanded equation (33), one finds

$$4c_2\delta = c_1^2[\epsilon^2-2\eta+a_2][4\epsilon-2\eta+2a_1-3a_2] \quad (38)$$

to the same degree of approximation, with

$$\begin{aligned} c_1a_1 &= 2\delta_c^{cr}c_3+6\kappa_F^{cr}\delta_c^{cr}+\delta(1-2\kappa_F^{cr}),\\ c_1a_2 &= \delta_c^{cr}c_3+2\kappa_F^{cr}\delta_c^{cr}+\delta(1-2\kappa_F^{cr}), \end{aligned} \quad (39)$$

in which δ_c and κ_F^{cr} terms, appearing in equation (33) and (34), taken at $\Delta_{pf} = \Delta_{pf}^{cr}(t'=0)$, are easily recognized. equation (38) determines $\epsilon(\eta)$, which,when inserted in equation (37) and equation (36) gives t and Δ_{pf} respectively.

The case $t' = 0$, $\delta = 0$ is considered first. As required, constants a_i vanish and the solutions of the conventional theory are recovered: $\epsilon(\eta) = \pm\sqrt{2\eta}$ and $t = 0$ for $\eta > 0$ and $2\epsilon = \eta$, $t^2c_2 = -t_0^2c_1^2\eta$ for $\eta < 0$, *i.e.* above and below BR point at $\eta = 0$. The upper and the lower branch $\pm\sqrt{2\eta}$ of the $t = 0$ parabola (37) correspond respectively to the limits $\delta = 0_\pm$ for the doping δ. At $t = 0$, $\delta = 0$ all the states enclosed by the two branches are possible since degenerate in energy $E = -\Delta_{pd}$ of equations (5) and (31), irrespectively on the value of Δ_{pf} (*i.e.* λ), they correspond to. Three solutions meet in the single $\eta = 0, \epsilon = 0$ point, which is thus, as emphasized here, the triple phase-transition point.

Taking in the next step finite $a_{1,2}$ in equations (37) and (38), but keeping $\delta = 0$, it can be easily seen that the zeros of two brackets in equations (38) meet at $2\hat{\eta} = a_2$ and $2\hat{\epsilon} = 2a_2 - a_1$. Omitting for the moment small $\kappa_F\delta_c$ terms in equation (39), it is found that three solutions of equation (38) meet again in the apex of $2a_2 - a_1 = 0$ of the $t = 0$ parabola (37), *i.e.* that to the leading order in δ_c the triple point nature of the $t' = 0$ BR transition is conserved. The BR point is only shifted in equation (35) to the position $2\hat{\eta} = a_2$ linearly in t'. Turning now to the doping dependencies, it is easily seen that the solution $\epsilon(\eta)$ of equation (38) is much more sensitive to the "external" δ, l.h.s. of equation (38), than to the "internal" δ entering this equation through a_1 and a_2 of equation (39). In the triple point itself, this leads to $\hat{\epsilon} \approx \delta^{1/3}$ and $t^2 \approx \delta^{2/3}$ with full electron-hole ($\delta \to -\delta$) symmetry.

The complete behavior $\epsilon(\eta) + 2\eta$ of equation (36) *vs.* δ is illustrated in Figure 8. Obviously this figure also applies to the $t' = 0$ situation putting $a_2 = 0$. Together with the observation that t vanishes above the BR point (at $2\hat{\eta} = a_2$) in whole $\delta = 0$ region, and it is finite otherwise, Figure 8 represents a phase diagram associated with E_0 of equation (31): the hole-doped and the electron-doped metallic phases, separated below the BR point by the $\delta = 0$, $t \neq 0$ line, meet in the triple point with the $\delta = 0$ insulating phase. Actually, the phase transition line is expected to become the crossover line for the quantity $\langle b_R^\dagger b_R\rangle$ in more advanced treatments which forbid the long-range order $\langle b_R^\dagger\rangle = \langle b_R\rangle = b_0 \neq 0$.

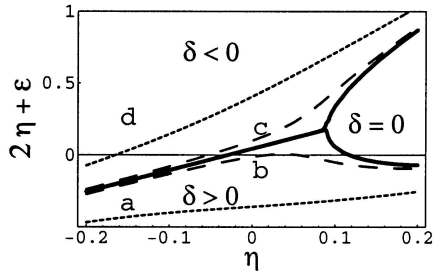

Fig. 8. Dependence of $2\eta + \epsilon$, *i.e.* Δ_{pf} on η, *i.e.* Δ_{pd} and on doping δ, in the neighborhood of the BR transition point. Solid line: $\delta = 0$, a: $\delta = 0.12$, b: $\delta = 0.01$ (dashed lines), c: $\delta = -0.01$, d:$\delta = -0.12$ (dotted lines).

Returning to the MFSB theory, as mentioned before, the terms $\kappa_F \delta_c$ are breaking at $\delta = 0$ local conduction band electron-hole symmetry and this is reflected now in equations (38) and (39). Indeed, at $\delta = 0$, $\hat{\epsilon} = 2a_2 - a_1$ differs from zero in the presence of $\kappa_F \delta_c$: the three solutions no longer meet in $\epsilon = 0$ apex of parabola (37). The low ϵ solution meets at $t = 0$ the δ_+ branch ($\hat{\epsilon} < 0$) of the parabola (37). This is now the point of the 0_+ second order transition. For $0 < \delta < \kappa_F \delta_c$, $\epsilon(\delta) - \hat{\epsilon} \sim \delta^{1/2}$, $t \sim \delta^{1/2}$. In contrast to that, for small negative δ the abrupt transition to the δ_- side is foreseen. Since physical $\kappa_F \delta_c$ is very small, these results, well beyond the accuracy of the existing numerical calculations, are mostly of the academic value, the main physical result of the present analysis thus being the conservation of the $t' = 0$ triple point nature of the BR transition to the leading order in t'.

It should be finally noted that the perturbative treatment of t' is consistent in the vicinity of BR transition provided that the corresponding δ_c^{cr} is smaller than unity, *i.e.* that $10|t'| < t_0$. This inequality is well in the spirit of the Emery model. However, remembering the particular role played in MFSB theory by $4|t'| < \Delta_{pf}^{cr}$ condition, a somewhat less conservative estimate $2|t'| < t_0$ for the qualitative applicability of the present analysis is obtained.

4.5 Intermediate perturbative range $t_0 < \Delta_{pd} < t_0^2/|t'|$ at small t'

When strong inequality $|t'| \ll t_0$ is assumed, the range of the applicability of the perturbative treatment of $|t'|$, *i.e.* of equation (33) and (34) extends from the vicinity of BR point, $\Delta_{pd} \approx t_0$ (*i.e.* $\eta < 1$), to $\Delta_{pd} \gg \Delta_{pd}^{cr}$, although not, as will be seen later below, to very large Δ_{pd}.

Equation (34) can be easily solved at $t = 0$ for $\Delta_{pf} \ll \Delta_{pd}$, *i.e.* for $\delta = 0_+$, to give

$$\Delta_{pf} = \frac{4t_0^2}{\Delta_{pd}}(c_1 + \delta_c c_3). \tag{40}$$

Essentially, weakly modified asymptotic behavior of $t' = 0$ theory [7] is recognized here, provided that δ_c of equation (28) is smaller than unity, *i.e.* for $\Delta_{pd} < t_0^2/|t'|$. Equation (33) gives then the usual $t \approx \Delta_{pf}\delta^{1/2}$ law.

On the other hand, Δ_{pf} of δ_- solution approaches Δ_{pd}, as easily seen from equation (34).

4.6 Asymptotic behavior at $|t'| > t_0^2/\Delta_{pd}$, Δ_{pd} large

In summary, the condition for validity of MFSB perturbative treatment of t' for the 0_+ CT branch is that bare O-O dispersion width $4|t'|$ is smaller than the width of $t' = 0$ bare copper band, t_0 close to BR transition and t_0^2/Δ_{pd} far above. For $\Delta_{pd} \approx t_0^2/|t'|$, Δ_{pf} of equation (40) becomes comparable to $4|t'|$, δ_c of equation (28) approaches unity, and the perturbative treatment of t', based on equation (27), breaks. The question then arises whether for $\Delta_{pd} > t_0^2/|t'|$, Δ_{pf} falls below $4|t'|$, which, according to our previous discussion requires $t \neq 0$, or remains above it, allowing $t = 0$ insulating state. Essentially related to the stability of $t = 0$ solution, this question can be discussed by replacing equation (27) by equation (21), non expanded in terms of t' and quadratic in t. Importantly, equation (21) insures the continuous transition from the regime (27), perturbative in t' to the regime perturbative in t.

The dominant contribution of the dispersion (21) to the cohesive energy comes from the states around **M** point, as apparent from Figure 2. On the contrary the states around μ are not important, *i.e.* E_0 is strongly dependent on $\widetilde{\Delta}$ and weakly dependent on μ, *i.e.* on δ. Expanding then equation (21) in $\mathbf{k}$ in the neighborhood of the **M** point, one finds immediately that E_0 is logarithmical in $\widetilde{\Delta}$,

$$E_0 \approx -\Delta_{pf}(1+\delta) - \frac{2\pi t^2}{|t'|}\log\frac{\Delta_{pf}}{\widetilde{\Delta}}. \tag{41}$$

Through MFSB equation (10) for 0_+ branch, this leads to $t = 0$ at

$$\widetilde{\Delta} = \Delta_{pf} - 4|t'| \approx 2|t'|\mathrm{e}^{-\frac{|t'|\Delta_{pd}}{4\pi t_0^2}}. \tag{42}$$

Equation (42) shows that Δ_{pf} remains above $4|t'|$. $t = 0$ is thus the consistent solution of $\delta = 0_+$ MFSB equations in the whole range $\Delta_{pd} > \Delta_{pd}^{cr}$.

In contrast to that, the asymptotic behavior $\Delta_{pf} \approx \Delta_{pd}$ of the 0_- branch is only weakly affected by t'.

Although $t = 0$ remains stable for large Δ_{pd}, t' leads to the qualitatively important modification of the CT behavior, replacing equation (40) for Δ_{pf} by equation (42). It should be remembered in this respect that Δ_{pf} of equation (40) represents the energy scale, which in the corresponding t-J model describes the site energy of both the singlet and the triplet states. It is this energy, which is qualitatively modified by t' in the MFSB approximation (42).

Exponential behavior of Δ_{pf} similar to equation (42) was previously proposed [22] for the 1d CuO t, t' model. It was also suggested there that MF theories are not sensitive to the dimensionality. However, the appropriate treatment of the band-dispersion shows that the result

obtained in [22], should actually be replaced by a power-law $\widetilde{\Delta} \sim t_0^2/\Delta_{pd}$, representing the signature of the dimensionality of the problem. This basically implies that the fact that Δ_{pf} saturates at the value of the oxygen bandwidth does not depend on the dimensionality of the problem, whereas the saturation law does. In addition to this, it should be noted that, in 2d situation, in order to have the saturation of Δ_{pf}, the anticrossing limit $\mathrm{sign}\Delta_{pf} = -\mathrm{sign}t' > 0$ should be chosen, while in the opposite case of band-touching, saturation is not expected. This justifies additionally careful analytical MFSB analysis of the 2d 3-band Emery model, carried out here.

Concerning now doping dependence of $\Delta_{pd} > t_0^2/|t'|$ solution, it is easy to verify that equations (8, 9) with equation (41), conserve $\delta \sim t^2$ structure analogous to that of equation (33), except that its perturbative nature in t requires now $t^2 < \widetilde{\Delta}\Delta_{pf}$ instead of $t < \Delta_{pf}$. As $\widetilde{\Delta}$ is exponentially small, $t \sim \delta^{1/2}$ behavior is reduced to very small doping δ.

For larger doping, equation (20) should be used instead of equation (21) in MFSB equations. This would answer the question whether Δ_{pf} crosses below $4|t'|$ at finite δ or whether it remains above $4|t'|$. In the former case, t is expected to reach the values close to t_0, while in the latter case it is likely to saturate on $|t'|$. Detailed discussion of this question is therefore desirable, but will be tackled upon here only in Section 5 through the fits of the experimental results.

4.7 Asymptotic behavior $\Delta_{pd} < 4.7t_0$, t' small

Turning now to the regime $\Delta_{pd} < \Delta_{pd}^{cr}$ at $|t'| < t_0$ and $\delta = 0$, shown in Figure 8, after linear decrease of Δ_{pf} with decrease of Δ_{pd} described by $\epsilon = 2\eta$ in equation (36), Δ_{pf} approaches $4|t'|$ again, heading towards its nonrenormalized value Δ_{pd}, this time at finite t. When t^2/t'^2 reaches $-\Delta_{pf}/2t'$ of equation (26), touching occurs in two upper bands, but equation (27) continues to hold for the lowest band ε_L, the only one important for MFSB renormalization. Δ_{pf} becomes smaller than $4|t'|$, but at $t \approx t_0$ so that t' acts perturbatively in terms of t'/t [23]: equation (27) is valid for $0 < \Delta_{pf} < 4|t'|$ and leads to $\Delta_{pf} = 0$ at $\Delta_{pd} = 1.5t_0 + t'$.

Actually, equation (27) as written, is valid even for $\Delta_{pf} < 0$ for the lowest (conduction) band ε_c (now ε_U, according to our notation). For any $|\Delta_{pf}| < t \approx t_0$, it is perturbative in t'/t_0 while for large negative Δ_{pf}, when $\Delta_{pf} \approx \Delta_{pd}$, $|\Delta_{pd}| > t_0$, the regime perturbative in t'/Δ_{pf} is reached again. In other words, equation (27), perturbative in t', is appropriate for the MFSB theory in the whole range $\Delta_{pd} < \Delta_{pd}^{cr}$ and can be used to solve analytically MFSB equations [16]. The dependencies on δ are non-critical here: for Δ_{pd} sufficiently below Δ_{pd}^{cr}, t/t_0 decreases [16,37] with $\delta > 0$.

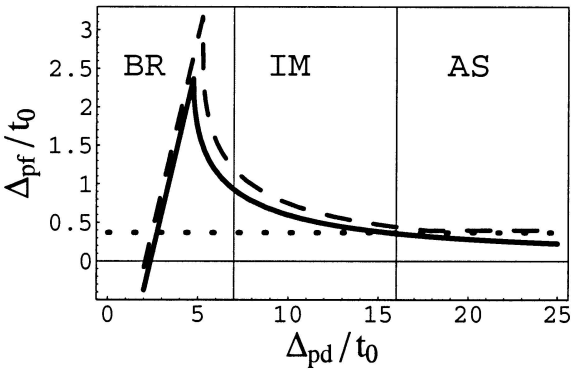

Fig. 9. Three different renormalization regimes depending on the ratio $4|t'|/\Delta_{pf}$ at zero doping δ; Solid line: $t' = 0$ case, dashed line: finite $t' < 0$ case with $4|t'|/\Delta_{pf} \ll 1$ in the neighborhood of the BR point. Dotted line represents the value of $4|t'|/t_0$. The plot implies that the perturbative treatment of t'/Δ_{pf} is justified around the BR point, while fails in the asymptotic (AS) regime. In the latter one, qualitative modification of the behavior of Δ_{pf} with respect to $t' = 0$ case is found, replacing asymptotical vanishing with the exponential saturation of Δ_{pf} at the value $4|t'|$ (the bandwidth of the oxygen band), suppressing thus insulator-metal transition at large Δ_{pd}/t_0.

4.8 Final remarks

Figure 9 summarizes the behavior of MFSB solutions at $\delta = 0_+$ for any $|t'| < t_0$, with $t' < 0$ above BR point, and arbitrary Δ_{pd}. The range of stability of the conducting phase is increased by $t' < 0$ (through $\hat{\eta} > 0$, to the larger values of Δ_{pd} with larger values of Δ_{pf}). The behavior of Δ_{pf} is more complex than the accompanying behavior of t. The latter raises smoothly and quickly below the shifted (rather than suppressed) BR transition towards its bare value t_0. In this range Δ_{pf} crosses first $4|t'|$ and then zero heading towards its bare value Δ_{pd}. On the other hand, above BR transition, Δ_{pf} remains above $4|t'|$ exponentially close to it for large Δ_{pd}/t_0: the necessary condition for the stability of the $t = 0$ solution is so fulfilled in the whole range above BR transition.

Noting however that in high-T_c superconductors $2|t'|$ is not expected to be much smaller than t_0, it is appropriate to comment briefly upon $t \approx 0$ regime in the opposite $2|t'| > t_0$ limit. Equation (41) describes then $t \approx 0$ behavior in whole range of Δ_{pd}/t_0. The BR point occurs at Δ_{pd} above $4|t'|$ with $\Delta_{pf} > 4|t'|$. The separation of $0_\pm$ solutions for Δ_{pf} in the vicinity of BR point, analogous to that of Figure 8 is governed by the logarithmic nature of E_0 in equation (41). For Δ_{pd} far above $4|t'|$ the logarithmic behavior of E_0 is important for the 0_+ branch, leading to the asymptotic behavior (42), while the asymptotic behavior $\Delta_{pf} \approx \Delta_{pd}$ of 0_- branch, the same as for $|t'| < t_0$, is again only weakly affected by t'.

Finally, before closing the discussion, it is physics-wise important to summarize briefly the case of doping behavior. Close to triple BR point, $t_\delta \sim |\delta|^{1/3}$ with the same coefficient for positive and negative δ. For $\Delta_{pd} > \Delta_{pd}^{cr}$ and

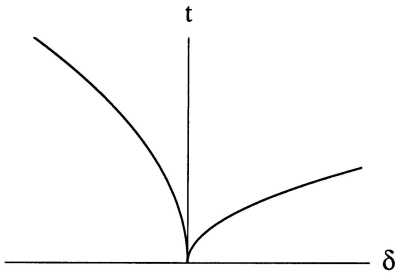

Fig. 10. Schematic doping dependence of the effective Cu-O overlap reflecting approximate electron-hole $|\delta|^{1/2}$ symmetry for $\Delta_{pd} > \Delta_{pd}^{cr}$, scales are given in the text.

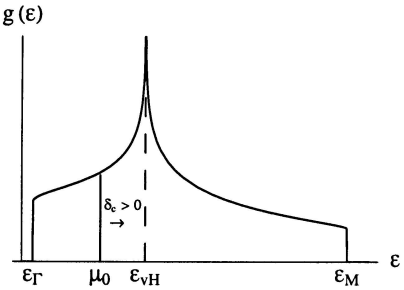

Fig. 11. Density of states of the lowest band ε_L reflecting the approximate secondary symmetry with respect to doping $\delta = \delta_c$, which brings μ from μ_0 at $\delta = 0$ to ε_{vH} at $\delta = \delta_c$.

$\delta < 0$, $t \approx t_0\sqrt{-\delta}$. Together with the corresponding result $t \approx \sqrt{\Delta_{pf}\widetilde{\Delta}\,\delta}$ described above for $\delta > 0$, this shows that MFSB approximation exhibits an approximate electron-hole ($\delta \to -\delta$) symmetry in its phase diagram with respect to $t = 0$ at $\delta = 0$, as illustrated in Figure 10.

In addition to this primary approximate symmetry, MFSB predicts secondary approximate e-h symmetry with respect to doping $\delta = \delta_c$, required to bring μ on the approximately symmetrical vH singularity in the density of states as illustrated in Figure 11, where δ_c is assumed positive. For $\delta < 0$, Δ_{pf} is much larger than for $\delta > 0$, except close to the BR point, and $|\delta_c|$ (δ_c positive or negative) is smaller for given t'. For small positive δ_c (*i.e.* $t' < 0$) doping $\delta < 0$ moves the Fermi energy farther from the vH singularity. Both approximate symmetries around $\delta = 0$ and $\delta = \delta_c$, well separated for appreciable $\delta_c > 0$, are observed in cuprates, and will be further discussed below.

5 Comparison with experiments

Several crucial aspects of the theory derived here can be compared straightforwardly with experiments. In the first place this concerns doping-dependent structure of the conducting band, measured in ARPES measurements. The corresponding MFSB fits [15,16] will be described in detail below. Although strikingly better than any other two-parameter fits, they cannot be considered as a final test in favor of MFSB theory because other strong-coupling regimes, in particular $t_0 < U_d < \Delta_{pd}$ (Hubbard limit), also result in strong doping-dependent renormalization of the conduction band.

Outright Hubbard limit, $\Delta_{pd} > U_d$ predicts however much stronger asymmetry in electron *vs.* hole doping (*e.g.* $\delta > 0$ is clearly forbidden at Hubbard $U_d \approx \infty$, unlike $\delta < 0$) than the $U_d > \Delta_{pd}$ $U_d \approx \infty$ case described here. The experimental phase diagram of the cuprates [28] is approximately symmetrical with respect to $\delta = 0$, favoring thus at large U_d the $U_d > \Delta_{pd}$ situation.

There is another related aspect of CT case which differs strongly from Hubbard limit, namely the existence of the resonant band for $\delta > 0$, well above dispersionless Cu level for Δ_{pd} large. In principle, this can be seen in high-energy spectroscopies, in particular in inverse photoemission.

Another qualitative difference between CT and Hubbard case concerns the interband transitions, which can be strongly renormalized in CT case in contrast to Hubbard limit. Existence of small interband scales, observable in principle by (MIR) optical and Raman spectroscopies [33,34], are therefore important in distinguishing between two limits. However, small interband scales predicted in CT case can mix with small scales associated with long and short-range AF and SC orders present in both CT and Hubbard cases. This requires very careful analysis which will be presented in separate papers [35,36], with the conclusion that they are mostly of the magnetic origin.

High-energy spectroscopies are usually used to determine the bare value of Δ_{pd}, associated with the dispersionless background according to equations (12) and (13), and U_d. It is found that [38] $U_d \approx 8-10$ eV and $\Delta_{pd} \approx 1-4$ eV, *i.e.* $U_d > \Delta_{pd}$.

With strong evidences in favor of CT case, local properties of the present MFSB solution can also be examined. As MFSB theory neglects magnetic (and SC) effects, only the behavior of the charge channel, *i.e.* of $\langle n^d\rangle$ and $\langle n^p\rangle$, $\langle n^d\rangle + 2\langle n^p\rangle = 1 + \delta$, is to be examined in this context. Very convenient local property for this purpose is NQR resonance, which measures the electric field gradients (EFGs) at the nuclear site. The EFGs depend strongly on the nature of the local electronic sites involved, and on their occupation. Apparently, the Cu resonance is particulary sensitive to $\langle n^d\rangle$; actually the resonant frequency increases linearly with $\langle n^d\rangle$ [37]. Experiments on $La_{2-\delta}Sr_\delta CuO_4$ (LSCO) and $YBa_2Cu_3O_{7-\delta}$ (Y123) show that Cu resonant frequency increases sharply with doping $\delta > 0$, smoothly through AF phase transition. As the first, this means that AF order affects weakly charges $\langle n^d\rangle$ and $\langle n^p\rangle$, as implicit in MFSB approach. As the second, this can be matched with the relation $\langle n^d\rangle = 1 - t^2/t_0^2$, either by assuming that $\langle n^d\rangle$ increases (*i.e.* t decreases) with δ, or assuming that the dependence of $\langle n^d\rangle$ on δ is weak, so that the other contributions to EFGs are more important. This rules out the vicinity of BR point $\Delta_{pd} \approx 4.74t_0(1 + 0.74\delta_c^{cr})$ (Fig. 8), where the dependence of t on doping is strong, but occurs well above BR point when the coefficient of the linear relation between t^2/t_0^2 and $\delta > 0$ becomes small: all doped holes simply go to

oxygen $2\langle n^p\rangle = \delta + t^2/t_0^2$. The resulting change in Cu resonant frequency was calculated before [39] and is in the excellent agreement with experiments. On the other hand, sufficiently below BR transition $\langle n^d\rangle$ increases (t decreases) with $\delta > 0$ in a way which can also explain [37] the behavior of Cu resonant frequency. The latter fit suggests that the additional hole is nearly equally shared between all three sites, as appropriate for $\Delta_{pf} \approx 0$.

NQR analysis leaves thus open two possibilities and to resolve the remaining dilemma, it is appropriate to resort to the ARPES data. While NQR measures l.h.s. of $\langle n^d\rangle = 1 - t^2/t_0^2$, ARPES measures its r.h.s. and it is important to find whether and when two sides are consistent. This is the question to be discussed now.

5.1 LSCO

Lanthanum system $La_{2-\delta}Sr_\delta CuO_4$ has an obvious advantage when compared to the others examined later, as it has only one CuO_2 layer in unit cell and it is therefore close to the theoretical model used here. The analyzed data [17,18] measure the evolution of the valence band and the corresponding FS with the doping, starting from underdoped $\delta \approx 0.05$ to overdoped $\delta \approx 0.3$ regime. These results point out that the shape of the FS changes with the doping. It is hole-like (dominant propagation along O-O axis) in underdoped regime ($\delta = 0.05; 0.1$), then passes through van Hove singularity close to the optimal doping ($\delta = 0.15$) and finally becomes electron-like (dominant propagation along Cu-O axis) in overdoped regime ($\delta = 0.22; 0.3$). The transition to the well-developed metallic regime can be associated with approaching to the vH energy. According to these fits, Luttinger's sum rule is obeyed, *i.e.* the enclosed surface of the BZ, normalized to 2 states per CuO_2 unit, is equal to $1 + \delta$.

The rotation of the propagation axes from O-O to Cu-O direction with doping implies that $t/|t'|$ increases sharply with doping. Further analysis of the observed Fermi surfaces requires either Δ_{pf} small, $\Delta_{pf} \ll 4|t'|$, or $\Delta_{pf} - 4|t'|$ small, $|\Delta_{pf} - 4|t'|| < 4|t'|$, corresponding roughly to Figures 5a and 2, respectively. As emphasized in Section 4.1, for $\Delta_{pf} < 4|t'|$ at $\delta \approx 0$, the system is below the BR transition, as clear from Figure 9 (valid for $4|t'| < t_0$).

This weakly renormalized regime (and even more the regime $4|t'| > t_0$) is associated with noncritical doping dependence on t at fixed t_0. The observed strong doping dependence of t can then be associated only with the one of t_0, starting from $t_0 < |t'|$ Such behavior of t_0 is not acceptable in the TB approximation.

The only regime which remains is $\widetilde{\Delta} = \Delta_{pf} - 4|t'|| \approx 0$, corresponding in particular to IM to AS regimes of Figure 9. For the interpretation of the NQR data, this regime puts the doped holes on the O-site, in agreement with equation (8) and [39]. The resulting detailed fits of the observed Fermi surfaces, together with the corresponding values of Δ_{pf}/t' and t/t' are shown in Figure 12. While the fits in the underdoped regime are only qualitatively significant because the localization and magnetic effects,

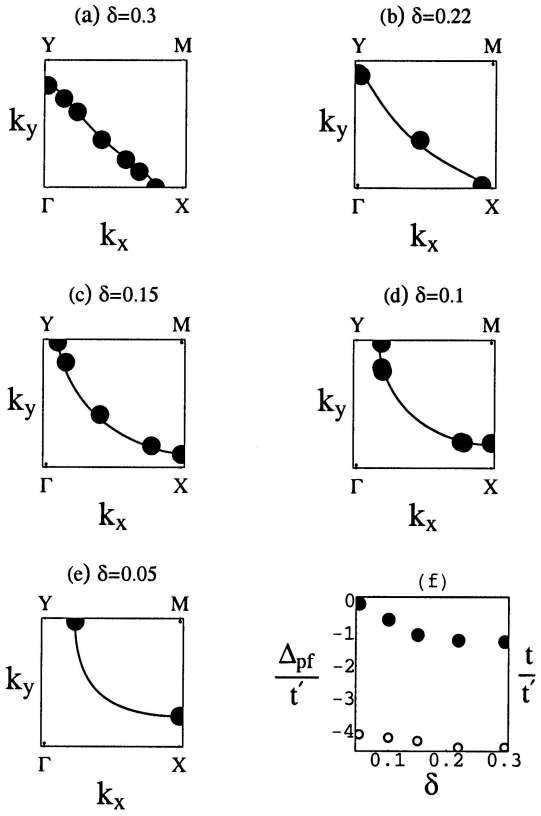

Fig. 12. (a–e) Experimentally measured Fermi surfaces for LSCO [18] (dots) and the three band model fits (solid). (f) fitting parameters in the regime of small $\widetilde{\Delta}$; circles: values of Δ_{pf}/t', dots: values of t/t'.

neglected in the MFSB approximation, are still important, it is interesting to note that Δ_{pf} is close to $4|t'|$ in optimal to overdoped regime. This indicates that Δ_{pf} saturates at $4|t'|$ for larger doping, the issue which, from the theoretical point of view, requires the use of equation (20) instead of equation (21) in the MFSB theory.

The IM/AS regime of Figure 9 also fits well the behavior of the hole spectrum, observed [18] below the Fermi energy. At small doping, a group of states is concentrated at 0.5 eV below the Fermi level. Upon doping, a part of these states moves gradually towards the Fermi level. The shape of the -0.5 eV resonance, as well as the one of the resonance at the Fermi level, is blurred, indicating no clear **k** dependence. Increasing the doping towards the optimum, the resonance at the Fermi level develops dispersion around **X** point. This evolution can be explained associating the –0.5 eV structure with the top of the oxygen band (with the reflection $\varepsilon \to -\varepsilon$, suitable for ARPES) as shown in Figure 13.

With doping the narrow resonant band is formed by transfer of the spectral weight, primarily from the oxygen band. According to equation (12) the number of the occupied states in this band is $(1 - \langle n^d\rangle)(1 + \delta)$. On $-\Delta_{pf}$, it is well separated from the background at $-\Delta_{pd} \approx -2$ eV, consistent with high-energy spectroscopies [38]. The value of Δ_{pf} can be determined from Figure 13: $\Delta_{pf} \approx 1.2$ eV

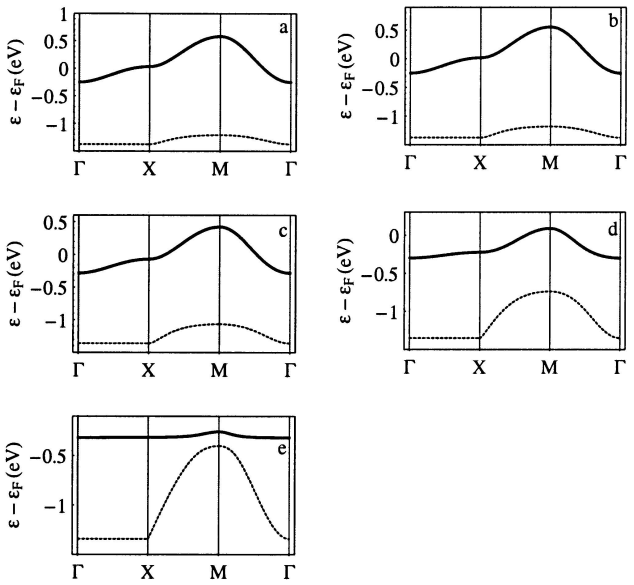

Fig. 13. Band-fits for the conducting band of LSCO of [18], corresponding to the Fermi surfaces of Figure 12.

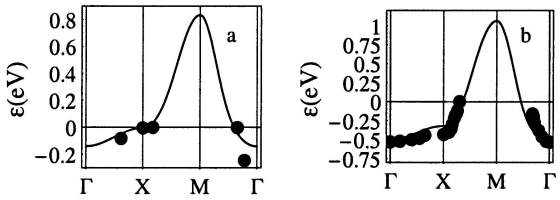

Fig. 14. Band-fits for the conducting band of Bi2212 of [25] with $\Delta_{pf} = 3.69$ eV, $t = 0.36$ eV, $|t'| = 0.9$ eV (a) and Y123 of [26] with $\Delta_{pf} = 2.7$ eV, $t = 0.36$ eV, $|t'| = 0.9$ eV(b).

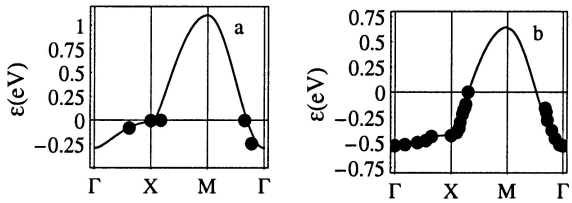

Fig. 15. Band-fits for the conducting band of Bi2212 of [25] with $\Delta_{pf} = t = 0.2$ eV, $|t'| = 0.35$ eV (a) and Y123 of [26] with $\Delta_{pf} = 0.06$ eV, $t = 0.06$ eV, $|t'| = 0.3$ eV(b).

and the values of the rest of the parameters can be obtained from the fits of Figure 13 as: $t \geq 0.6$ eV for $\delta = 0.3$, $|t'| \approx 0.3$ eV. This set of parameters is quite satisfactory from the physical point of view.

Qualitatively similar picture is obtained from $U_d = \infty$ NCA [31] and $U_d = 2$ eV DMFT [10] calculations, which also lead to the separation between the resonant band at $\varepsilon_f \approx \varepsilon_p$ and the background (lower Hubbard band [10]) at ε_d. As in the MFSB approximation, $t' < 0$ (t' is replaced by $-t'$ in convention of [10]) reduces the optical gap between the resonant band and the background.

5.2 Bi2212 and Y123

The analysis of the band-structure in LSCO is now followed by the the analysis of the ARPES data obtained for $Bi_2Sr_2CaCuO_{8+\delta}$ (Bi2212) [25] and $YBa_2Cu_3O_{7-\delta}$ (Y123) [26], having two CuO_2 layers in unit cell. In both of these systems the FS is hole-like in the whole range of doping. This reveals one of the long-standing questions in the interpretation of ARPES data: the evolution of the FS does not obey the Luttinger sum rule. Our model, for infinite U_d, consisting only of one CuO_2 layer cannot explain straightforwardly this result. It can only be pointed out, as the first, that the inter-layer couplings might account for this effect, keeping the conducting band at constant doping, transporting the added holes to the other one, above Fermi energy. Secondly, Luttinger's sum rule is modified at finite U_d, and this can thus point towards such effects. Finally, the phase separation, *e.g.* of the $0_\pm$ kind, or similar, may produce the domains of coherence for the bands filled up to the vH singularity.

The experimentally measured shapes of the conducting bands in Bi2212 and Y123, as well as the corresponding Fermi surface, reveal oxygen-like character, *i.e.* hole-like Fermi surface implies the domination of $|t'|$. In the slave-boson model used here, this can be achieved in basically two ways. As the first, saturation regime of band-parameters can be used, assigning oxygen-like features to the copper band and keeping $\Delta_{pf} \approx 4|t'|$. These fits are given in Figure 14.

In Bi2212, $\Delta_{pd}/4|t'| \approx 1$, but in Y123 smaller value was taken in order to fit more accurately experimental data. This reflects the fact that the conducting band in Bi2212 is flattened in the vicinity of the vH singularity, which can be however alternatively explained with AF fluctuations [2,36]. Unlike Bi2212, conducting band of Y123 is strongly dispersive throughout the Brillouin zone and essentially reflects oxygen-like symmetry. Nevertheless, slave-boson fits of Figure 14, where the value of Δ_{pf} was kept comparable to the value of $4|t'|$, could not reproduce equally well all the experimental points. Therefore, the alternative set of parameters were used to fit the same data, shown in Figure 15 where $4|t'| \geq \Delta_{pf}, t$ in Bi2212 and $4|t'| \gg \Delta_{pf}, t$ in Y123.

From the slave boson point of view, these values of effective parameters can be obtained in two ways. As the first, the values of bare parameters could be such that the lowest band is basically oxygen-like, *i.e.* $|t'| \gg \Delta_{pf}$. Then the renormalization is weak $\Delta_{pf} \approx \Delta_{pd}$, $t \approx t_0$, hence the ratio of the parameters does not change with doping. This, however does not agree with the large values of Δ_{pd} determined from high-T_c spectroscopies [38]. As the second, the copper band could cross the oxygen band in the IM/AS region of Figure 9 when finite doping is added. As mentioned at the end of Section 4.6, t should then saturate with doping at t_0. Higher values of t could then be expected, unless $2|t'| \gg t_0$, which is unlikely. This, however, depends on how fast the saturation of t is achieved upon doping, the question which cannot be answered without carrying out the MFSB theory, using equation (20) instead of equation (21).

6 Conclusion

In conclusion, the 3-site Emery model with Cu-O and O-O hoppings, t_0 and t' respectively, the bare Cu-O CT gap Δ_{pd} and large interaction U_d on the Cu-site is treated here within the mean field slave boson approximation. The results are obtained analytically for arbitrary values of t'/t_0 and Δ_{pd}/t_0. The additional assumption for the insulting phase, $t' < 0$, is adequate for the high-T_c cuprates.

Three aspects of the resulting singular behavior are considered: the singular dispersion properties of the three bands in the whole parameter-space of renormalized band parameters, the phase transition singularities in relation between renormalized and bare parameters and, with reference to the companion paper, the singularity of the d-electron spectral density, associated with the formation of the resonant band.

A number of new results is obtained this way: the band-touching *vs.* band-anticrossing issue in the dispersion of three-bands is entirely elucidated by determining analytically the range of parameters, wider than known before, in which the touching occurs. Anticrossing, rather than touching is found to be important for the high-T_c cuprates.

The solution of the mean field slave boson equations in the anticrossing regime for zero doping leads to important new results: at large Δ_{pd} the effective CT energy saturates exponentially at the value $4|t'|$, rendering stability to the insulating state. If $2|t'| < t_0$, the range of stability of the insulating state extends from large Δ_{pd} to Δ_{pd} of the order of t_0. The BR transition keeps its triple point nature linearly in t', *i.e.* its full electron-hole symmetry is conserved. The (logarithmically small) departure of the Fermi level from the vH singularity, induced by t' breaks explicitly the electron-hole symmetry and removes the $t' = 0$ triple point nature of the BR point.

The electron-hole symmetry appears also at finite positive or negative doping. Close to the BR point the symmetry is nearly complete at t' finite but small, $2|t'| < t_0$, whereas for in the insulating phase it is only approximate. In the latter case, the symmetry breaking,which exists already at $t' = 0$, comes from the interaction, but it is modified by finite t'; in any case doped holes go to O-sites, while doped electrons go to Cu-sites.

This picture is finally compared to the experiments on high-T_c cuprates, ARPES in particular, associating the observed single particle spectral density close to the Fermi level with the resonant band. The idea of hole doping to the O-sites is consistent with the NQR data for LSCO and Y123. ARPES data in LSCO agree well with the picture of the resonant band building its intensity by the transfer of the oxygen states to the Fermi level, on satisfying the Luttinger sum rule. The effective mass in this band is given by the O-O hopping, large with respect to the strongly renormalized Cu-O hopping. This, nearly covalent behavior differs essentially from the heavy-fermion limit, obtained in $t' = 0$ case. The data on B2212 and Y123 also require dominant t', but the Luttinger sum rule is not satisfied.

Several questions thus remain to be answered in the future. The most fundamental seems to be related to the breakdown of the Luttinger sum rule in Bi2212 and Y123, if it is related to the moderate values of U_d on Cu-site. Even for U_d large, the question of moderate doping is worth further investigation. Above all, after achieved the renormalization by a factor of ten of the bare single-particle energy scales to the effective values (from 1eV to 0.1 eV), the further step (from 0.1eV to 0.01 eV), using the effective interactions between auxiliary particles, leads sight into the middle of the high-T_c problem.

We thank Ph. Nozières, J. Friedel and L. Gor'kov for many useful discussions. This work was supported by Croatian Ministry of Science under the project 119-204.

References

1. E.W. Carlson, V.J. Emery, S.A. Kivelson, D. Orgad, `cond-mat 0206217`, review chapter to appear in *The Physics of Conventional and Unconventional Superconductors* edited by K.H. Bennemann, J.B. Ketterson (Springer-Verlag, 2003)
2. J. Friedel, M. Kohmoto, Eur. Phys. J. B **30**, 427 (2002)
3. S. Barišić, Int. J. Mod. Phys. B **15**, 2439 (1991)
4. M.S. Hybertsen, E.B. Stechel, M. Schulter, D.R. Jennison, Phys. Rev. B **41**, 11068 (1990)
5. P.W. Anderson, *The Theory of Superconductivity in the High T_c Cuprates* (Princeton, New Jersey), 1997
6. V.J. Emery, Phys. Rev. Lett. **58**, 2794 (1987)
7. B.G. Kotliar, P.A. Lee, N. Read, Physica C **153-155**, 538 (1989)
8. G. Esirgen, N.E. Bickers, Phys. Rev. B **57**, 5376 (1998) and references therein
9. M. Guerrero, J.E. Gubernatis, Phys. Rev. B **57**, 11980 (1998) and references therein
10. M.B. Zölfl, Th. Maier, Th. Prusche, J. Keller, Eur. Phys. J. B **13**, 47 (2000) and references therein
11. S.E. Barnes, J. Phys. F **6**, 1375 (1976)
12. G. Kotliar, A.E. Ruckenstein, Phys. Rev. Lett. **57**, 1362 (1986)
13. Ju.H. Kim, K. Levin, A. Auerbach, Phys. Rev. B **39**, 11633 (1989)
14. F.C. Zhang, T.M. Rice, Phys. Rev. B **37**, 3759 (1987)
15. I. Mrkonjić, S. Barišić, `cond-mat/0103057` (2001)
16. I. Mrkonjić, Ph.D. thesis, University of Zagreb, 2003
17. A. Ino, C. Kim, M. Nakamura, T. Yoshida, T. Mizokawa, Z.-X. Shen, A. Fujimori, T. Kakeshita, H. Eisaki, S.J. Uchida, Phys. Rev. B **62**, 4137 (2000)
18. A. Ino, C. Kim, M. Nakamura, T. Yoshida, T. Mizokawa, Z.-X. Shen, A. Fujimori, T. Kakeshita, H. Eisaki, S.J. Uchida, Phys. Rev. B **65**, 94504 (2002)
19. C.A.R. Sa de Melo, S. Doniach, Phys. Rev. B **41**, 6633 (1990)
20. P.S. Riseborough, P. Hanggi, Phys. Rev. B **47**, 11540 (1993)
21. H. Kaga, T. Saikawa, A. Ferraz, P. Brito, Phys. Rev. B **50**, 13942 (1994)

22. M. Grilli, B.G. Kotliar, A.J. Millis, Phys. Rev. B **42**, 329 (1990)
23. I. Mrkonjić, S. Barišić, `cond-mat/0211128` (2002)
24. A.A. Abrikosov, J.C. Campuzano, K. Gofron, Physica C **241**, 73 (1993)
25. M.R. Norman, M. Randeria, H. Ding, J.C. Campuzano, Phys. Rev. B **52**, 615 (1995)
26. M.C. Shabel, C.-H. Park, A. Matsuura, Z.-X. Shen, D. A. Bonn, Ruixing Liang, W.N. Hardy, Phys. Rev. B **57**, 6090 (1998)
27. M.C. Shabel, C.-H. Park, A. Matsuura, Z.-X. Shen, D.A. Bonn, Ruixing Liang, W.N. Hardy, Phys. Rev. B **57**, 6107 (1998)
28. A. Damascelli, Z-X Shen, Z. Hussain, Rev. Mod. Phys. **75**, 473 (2003)
29. D.I. Golosov, A.E. Ruckenstein, M.L. Horbach, J. Phys. Cond. Matt. **10**, L229 (1998)
30. E. Tutiš, Ph.D. thesis, University of Zagreb (1994)
31. H. Nikšić, E. Tutiš, S. Barišić, Physica C **241**, 247 (1995)
32. D.Y. Xing, M. Liu, C.D. Gong, Phys. Rev. B **44**, 12525 (1991)
33. S. Uchida, T. Ido, H. Takagi, T. Arima, Y. Tokura, S. Tajima, Phys. Rev. B **43**, 7942 (1991)
34. S.L. Cooper, D. Reznik, A. Kotz, M.A. Karlow, R. Liu, M.V. Klein, W.C. Lee, J. Giapintzakis, D.M. Ginsberg, B.W. Veal, A.P. Paulikas, Phys. Rev. B **47**, 8233 (1993)
35. I. Kupčić, S. Barišić, unpublished
36. D.K. Sunko, S. Barišić, *Seventh International Conference on Materials and Mechanism of Superconductivity and High-Temperature Superconductors, May 25-30 2003, Rio de Janeiro, Brasil*
37. I. Kupčić, S. Barišić, E. Tutiš, Phys. Rev. B **57**, 8590 (1998)
38. N.M. Plakida, *High-Temperature Superconductivity* (Springer-Verlag, Berlin, Heidelberg, 1995)
39. R.L. Martin, Phys. Rev. Lett. **75**, 744 (1995)